12th HSTAM International Congress on Mechanics
Thessaloniki, Greece, 22 – 25 September 2019

ANALYTICAL, NUMERICAL AND EXPERIMENTAL ANALYSIS OF THE VIBRATIONAL BEHAVIOUR OF ADHESIVELY COMPOSITE DOUBLE-LAP JOINTS

Elias A. Salloum[1,2], Georges E. Challita[1], Akram Alhussein[3], and Khaled Khalil[1,4]

[1]MMC team, CRSI
Lebanese University - Faculty of Engineering
Campus Hadath, Beirut, Lebanon.
e-mail: salloum.elias@u-picardie.fr georges.challita@ul.edu.lb khkhalil@ul.edu.lb

[2] Laboratoire des Technologies Innovantes, LTI -EA 3899
Université de Picardie Jules Verne, Amiens 80025, France

[3]ICD-LASMIS
Université de Technologie de Troyes
CNRS, Antenne de Nogent, Pôle Technologique de Sud-Champagne 52800 Nogent, France
e-mail: akram.alhussein@utt.fr

[4]Université de Nantes - Ecole Centrale Nantes
Institut de Recherche en Génie Civil et Mécanique (GeM)
UMR CNRS 6183, Equipe Etat Mécanique et Microstructure
58 rue Michel Ange, BP 420, 44600 Saint-Nazaire, France

Keywords: Double-lap joints, Adhesion, Modal analysis, Impulse Excitation Technique, Finite Elements.

Abstract. *In this paper an analytical model based on finite element energy formulation that calculates free vibration frequencies of cantilevered-free laminated double lap bonded joints is established. 8-noded serendipity element with quadrature Gaussian formula was adopted. This model was validated using 3D finite element model through ANSYS Workbench. The results have shown good agreement for steel and composite while it was not the case for polymeric substrates. Moreover, an experimental procedure for analysing the vibrational response of adhesively composite double lap joints is presented in this paper. The Impulse Excitation Technique (IET) has been adopted in order to measure the resonant frequencies. Two types of substrates were examined: steel and orthotropic glass-polypropylene composite and the adhesive used is a resin/epoxy constituent. Three different substrates thicknesses and three different overlap lengths were examined. Then, the experimental results were compared with numerical simulations using 3D finite element model through ANSYS Workbench. The results have shown good agreement between both models. Finally, the analytical model was applied to compare the experimental results in the scope of a parametric study towards the influence that some geometrical and mechanical properties of the adherents have on the vibrational response of the structure.*

1 INTRODUCTION

In the last few decades, light weight structures were constituting the main target for both industrials and researchers since such structures contribute in the reduction of carburant consumptions and hence cost reduction and green environment. Bonded joints are among the light weight structures used in many applications especially in transportation and construction fields. Such structures may be subjected to many types of mechanical loadings; vibration of such structures is actually the main concern of many researchers.

It is known that single lap joint (SLJ) is the most used geometry to investigate bonded joints in vibration; many analytical models based on discretization were developed in the previous century to study free vibration of single lap joint structures [1-5]. However, in the present century, numerical simulations constitute the main tool for any experimental validation. One can cite the work of He and Oyadiji [6] who examined the variation of natural frequencies, transverse mode shapes and strength of a single cantilevered lap joint in terms of adhesive mechanical properties using ABAQUS software. He [7] was interested in free vibration of SLJ under torsion: he carried out a parametric study by changing the values of adhesive's mechanical properties where he found that only Young's modulus has the main influence on the resonant frequencies. Du and Shi [8] investigated also the effect of Young's modulus of the adhesive and established a relation between vibration and fatigue of a steel-aluminum single lap joint. Samaratunga et al. [9] have studied analytically the wave propagation in a composite single lap beam and validated it numerically using ABAQUS for simulations. Harmonic force applied to single lap joint was the main

concern of Vaziri et al. [10]; they investigated analytically the dynamic response of a void-defected SLJ under an out-of-plane harmonic force where they found only an influence of the location of the void and not of its size.

Less works could be cited where other geometries were adopted. Rao and Zhou [11] have established governing equations for transverse and axial vibration of tubular joints where the effect of materials and geometry on modal loss factor and resonant frequencies was examined. Vaziri and Nayeb-Hashemi [12] have applied the same concept as in Vaziri et al. [10] but for axial harmonic loading on tubular joint geometry; also parametric study was carried out for elastic and viscoelastic adhesive. Free vibration of stiffened cylindrical shells have constituted the main concern of Quing et al. [13] where a semi-analytical model was established. It was applicable to piezolaminated and patched plates and shells. Challita and Othman [14] have chosen the double lap joint geometry (DLJ) to establish a closed-form analytical model based on the modified shear lag model to determine the shear stress field in the adhesive layer under an axial harmonic loading. In the same context, Al-Mitani and Othman [15] have extended this study for a viscoelastic adhesive; they have conducted also a parametric analysis to study the influence of shear's modulus, thickness and loss factor of the adhesive and many geometrical and mechanical parameters of the substrates on the first three resonant frequencies. Jiang and Heyliger [16] have applied continuous polynomial and trigonometric functions to investigate the effect of the thickness on non-dimensional frequencies of magnetoelectroelastic plates under many cases of boundary conditions.

In the present paper, free vibration of a fixed-free DLJ structure is investigated analytically, numerically and experimentally. This geometry was rarely tackled in the previous works although its simplicity and symmetry. Two substrates' materials are considered: steel and orthotropic glass/epoxy laminate. For each substrate, three thicknesses configurations and three overlap lengths values are considered. On one hand, the energy formulation based discretization was used to develop the analytical model; on the other hand, the Impulse Excitation Technique is the experimental instrument used to measure the natural frequencies while ANSYS Workbench is the numerical tool adopted for validation.

2 SEMI-ANALYTICAL METHOD

2.1 Specimen description

The specimen's geometry adopted in this study is the double lap joint shown in fig. 1. The structure is constituted of three rectangular plates of length L and width b, bonded together. The middle plate of thickness t_2 is shifted horizontally with respect to the two other cantilevered plates of thickness t_1. The other end of the middle plate is free. Bonding is applied between the upper and the middle plates and between the middle and the lower plates with a thickness t_a. The overlap bonding length is a.

2.2 Assumptions

In this study, the following assumptions are considered: (1) Small deformations, (2) the adhesive is free from anti-plane stress state: $\sigma_{ax} = \sigma_{ay} = \tau_{axy} = 0$, (3) all materials used are homogeneous and linearly elastic, (4) the peel and shear stresses along the thickness direction in the adhesive layer are assumed uniform and (5) the transverse normal modulus of adhesive is much lower than that of the adherents so that the transverse normal deformation of the adherents is negligible in comparison with that of the adhesive.

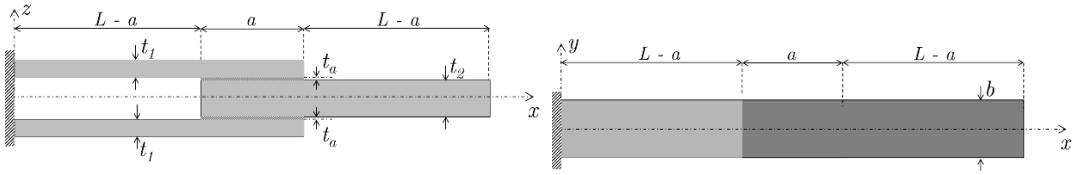

Figure 1. A Double lap-jointed cantilevered structure.

2.3 Boundary conditions

The upper and the lower plates are fixed from one end. Thus, the boundary conditions are considered as equality constraints to the free vibration problem as follows:

$$\{\delta_i(0,y,t)\} = 0_{5,1} \qquad i = 1,3 \tag{1}$$

$$\text{Where } \{\delta_i(x,y,t)\}^T = \left[u_i^0, v_i^0, w_i, \psi_{ix}, \psi_{iy}\right]_{1\times 5} \tag{2}$$

is the displacement vector at any point in the plane (x,y) at time t, with 5 displacement components for laminated plates: 3 linear and 2 angular: u_i^0 and v_i^0 are the mid-plane linear displacement components along x and y, w_i is the linear displacement component along z, and ψ_{ix} and ψ_{iy} are the angular displacement components about x and y axis for the i^{th} plate.

2.4 Energy formulation

The total potential energy of the system consists of contributions from the 3 plates: upper (1), middle (2) and lower (3) plates,U_1, U_2 and U_3 respectively, the adhesive shear and normal strain between the plates 1 and 2, U_{a12} and between the plates 2 and 3, U_{a23} [3]. Similarly, the total kinetic energy T is the sum of the kinetic energies: T_1, T_2 and T_3 of the three plates respectively and T_{a12} of the adhesive layer between the plates 1 and 2, T_{a23} of the adhesive layer between the plates 2 and 3.

2.4.1 Strain energy of a plate

The strain vector of the i^{th} plate $\{\varepsilon_i\}$ is expressed as follows,

$$\{\varepsilon_{ix}\}^T = \begin{pmatrix} \varepsilon_{ix}^0 & \varepsilon_{iy}^0 & \gamma_{ixy}^0 & \kappa_{ix} & \kappa_{iy} & \kappa_{ixy} & \gamma_{ixz} & \gamma_{iyz} \end{pmatrix} \tag{3}$$

where ε_{ix}^0 and ε_{iy}^0 are the axial strain components along x, y axis, κ_{ix} and κ_{iy} are the bending strain components along x and y axis, κ_{ixy} is the twisting component along xy plane and $\gamma_{ixy}^0, \gamma_{ixz}$ and γ_{iyz} are the shear strain components along xy, xz and yz planes respectively.

The strain vector is related to the displacement vector defined in equation (2) as follows,

$$\{\varepsilon_i\}^T = \begin{pmatrix} \frac{\partial}{\partial x} & 0 & \frac{\partial}{\partial y} & 0 & 0 & 0 & 0 & 0 \\ 0 & \frac{\partial}{\partial y} & \frac{\partial}{\partial x} & 0 & 0 & 0 & 0 & 0 \\ 0 & 0 & 0 & 0 & 0 & 0 & \frac{\partial}{\partial x} & \frac{\partial}{\partial y} \\ 0 & 0 & 0 & \frac{\partial}{\partial x} & 0 & \frac{\partial}{\partial y} & 1 & 0 \\ 0 & 0 & 0 & 0 & \frac{\partial}{\partial y} & \frac{\partial}{\partial x} & 0 & 1 \end{pmatrix} \begin{pmatrix} u_i^0 \\ v_i^0 \\ w_i \\ \psi_{ix} \\ \psi_{iy} \end{pmatrix}^T = [d]^T\{\delta_i\}^T \tag{4}$$

We define the following stiffness matrix$[C^i]$,

$$[C^i] = \begin{pmatrix} A_{11}^i & A_{12}^i & A_{16}^i & B_{11}^i & B_{12}^i & B_{16}^i & 0 & 0 \\ A_{12}^i & A_{22}^i & A_{26}^i & B_{16}^i & B_{22}^i & B_{26}^i & 0 & 0 \\ A_{16}^i & A_{26}^i & A_{66}^i & B_{16}^i & B_{26}^i & B_{66}^i & 0 & 0 \\ B_{11}^i & B_{12}^i & B_{16}^i & D_{11}^i & D_{12}^i & D_{16}^i & 0 & 0 \\ B_{12}^i & B_{22}^i & B_{26}^i & D_{12}^i & D_{22}^i & D_{26}^i & 0 & 0 \\ B_{16}^i & B_{26}^i & B_{66}^i & D_{16}^i & D_{26}^i & D_{66}^i & 0 & 0 \\ 0 & 0 & 0 & 0 & 0 & 0 & A_{44}^i & A_{45}^i \\ 0 & 0 & 0 & 0 & 0 & 0 & A_{45}^i & A_{55}^i \end{pmatrix} \tag{5}$$

Where the constants $\left(A_{jk}^i, B_{jk}^i, D_{jk}^i\right)$ are defined as

$$\left(A_{jk}^i, B_{jk}^i, D_{jk}^i\right) = \sum_{m=1}^{n_i} \int_{z_m-1}^{z_m} Q_{jk}^{im}(1, z, z^2)\, dz \quad j,k = 1,2,6$$

$$A_{jk}^i = \sum_{m=1}^{n_i} \int_{z_m-1}^{z_m} K Q_{jk}^{im}\, dz \quad j,k = 4,5 \ \text{and} \ K = \frac{5}{6} \ [3]$$

z_{m-1} and z_m are the distances measured from the mid-plane of the total structure to the bottom and top surfaces of the m^{th} layer for the upper adherent ($i = 1$), the middle adherent ($i = 2$) and the lower adherent ($i = 3$) as shown in Figure 2. Q_{jk}^{im} are the reduced stiffnesses at m^{th} layer of the plate. In the case of isotropic material, m is equal to 1.

Hence, the strain energy in the i^{th} laminated plate is expressed as follows [3]:

$$U_i = \frac{1}{2} \int_{R_i} \{\varepsilon_i\}^T [C^i] \{\varepsilon_i\} dx dy \tag{6}$$

2.4.2 Strain energy of an adhesive layer between two plates

A bonded plate includes the layers of adherent and the adhesive layer, in which the bonded region may be viewed as a sandwich structural element (Lin and Ko [17]). From assumptions (2) and (4) there are only three stress components and their associated strain components in the adhesive with relations as

$$\tau_{axz} = G_a \gamma_{axz}(x,y,t) \qquad \tau_{ayz} = G_a \gamma_{ayz}(x,y,t) \qquad \sigma_{az} = E_a \varepsilon_{az}(x,y,t) \quad (7,8,9)$$

where the shear modulus G_a and the Young's modulus E_a are constant and the subscript a denotes adhesive. Using continuity conditions in the x and y directions along the interfaces between adherents and the adhesive at $z = t_a + d_i$ and $z = d_i$ we get,

$$\gamma_{axz}^{ij} = \frac{1}{t_a}(u_i^0 - u_j^0 + h_i\psi_{ix} + h_j\psi_{jx}) \quad (10)$$

$$\gamma_{ayz}^{ij} = \frac{1}{t_a}(v_i^0 - v_j^0 + h_i\psi_{iy} + h_j\psi_{jy}) \quad (11)$$

where $h_i = -\frac{t_i}{2} + d_i, h_j = -\frac{t_j}{2} + d_j$ and $d_i$and $d_j$denote the distances measured from the mid plane of the structure to the top and bottom of the adhesive between the $i^{th}$and j^{th} plates as shown in fig. 2.

The potential energy corresponding to the adhesive between the i^{th} and the j^{th} plates is obtained from the superposition of the shear and normal strain energies as follows (Ko et al. [3]):

$$U_{aij} = \frac{1}{2}t_a G_a \int_{R_a}(\gamma_{axz}^{ij\ 2} + \gamma_{ayz}^{ij\ 2})dxdy + \frac{1}{2}\frac{E_a}{t_a}\int_{R_a}\left(w_i - w_j\right)^2 dxdy \quad (12)$$

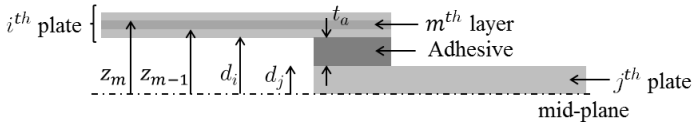

Figure 2. Distances from the mid-plane of the double lap joint.

2.4.3 Kinetic Energy of a plate and adhesive layer between two plates

The kinetic energy of the i^{th} plate and the adhesive between the i^{th} and the j^{th} plates are

$$T_i = \frac{1}{2}t_i\int_{R_i}\rho_i(\dot{u}_i^2 + \dot{v}_i^2 + \dot{w}_i^2)dxdy \qquad T_{aij} = \frac{1}{2}t_a\int_{R_a}\rho_a\left(\dot{u}_{aij}^2 + \dot{v}_{aij}^2 + \dot{w}_{aij}^2\right)dxdy \quad (13, 14)$$

where ρ_i and ρ_a are the densities of the i^{th} plate and the adhesive respectively and the average displacements of adhesive layer between the i^{th} and j^{th} plates (Ko et al. [3]) are

$$u_{aij} = \frac{1}{2}\left(u_i + u_j\right) + \frac{1}{4}, \qquad v_{aij} = \frac{1}{2}\left(v_i + v_j\right) + \frac{1}{4}\left(t_i\psi_{iy} - t_j\psi_{jy}\right) \text{ and } w_{aij} = \frac{1}{2}\left(w_i + w_j\right) \quad (15, 16, 17)$$

2.5 Finite element discretization

The problem described in the continuous domain is now discretized; the system is divided into isoparametric, 8-noded serendipity elements with first order shear deformation for each plate and each adhesive layer, using the finite element method (FEM), by transforming the physical coordinates (x, y) into local coordinates (ξ, η) as shown in figures 3 and 4. The size of the elements is selected based on a convergence test in order to compromise between the precision and the speed of resolution. Shape functions developed for 8-noded serendipity elements are used to discretize the domain. Hence, a variable u can be expressed using the nodal relationship:

$$u = \sum_{k=1}^{8} N_k u_k \quad (18)$$

where u_k is the variable's value at node k.

Hence, the nodal relationship is applied to the displacement components as follows,

$$u_i^0 = \sum_{k=1}^{8} N_k u_{ik}^0 \qquad v_i^0 = \sum_{k=1}^{8} N_k v_{ik}^0 \qquad w_i = \sum_{k=1}^{8} N_k w_{ik}$$
$$\psi_{ix} = \sum_{k=1}^{8} N_k \psi_{ixk} \qquad \psi_{iy} = \sum_{k=1}^{8} N_k \psi_{iyk}$$

Then, adopting the Gaussian quadrature formulas, mass and stiffness matrices can be derived for each element. Later, the global mass and stiffness matrices shall be obtained by assembling the elementary matrices with respect to the nodes displacement components, in order to calculate the natural frequencies corresponding to each mode in the discretized domain.

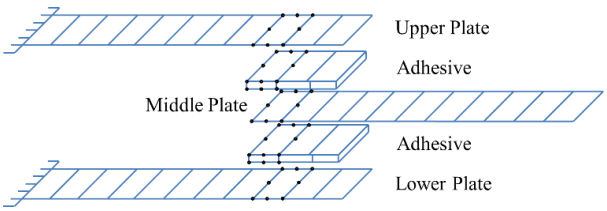

Figure 3. 8-noded finite element idealizations of double lap-joints.

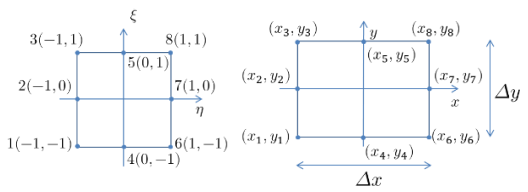

(a)

Figure 4. A schematic of the noded serendipity element with (a) local coordinates and (b) physical coordinates.

2.5.1 Plates Stiffness Matrices

To derive the stiffness matrix of each plate, one must first adopt the Gaussian quadrature formula by expressing the potential energy in the following form:

$$U_i = \frac{1}{2}\{\delta_i\}^T [K_i]\{\delta_i\} \tag{19}$$

Then, using the nodal displacement relationship in eq (18) applied on strain-displacement relation in eq (4), eq (6) is discretized as follows

$$U_i = \frac{1}{2}\{\delta_i\}^T \left(\int_{-1}^{1}\int_{-1}^{1}[B_i]^T[C^i][B_i]\ \det[J]d\xi\ d\eta\right)\{\delta_i\} \tag{20}$$

where J is the Jacobian matrix which is used to transform the physical coordinates $(x,\ y)$ to the curvilinear coordinates (ξ, η) and $[B_i]$ is constructed using the shape functions for 8-nodes serendipity element.

Hence, the stiffness matrix of the i^{th} plate can be expressed as,

$$[K_i] = \int_{-1}^{1}\int_{-1}^{1}[B_i]^T[C^i][B_i]\,det[J]\,d\xi\ d\eta \tag{21}$$

2.5.2 Adhesive Stiffness Matrices

From strain and nodal displacement relationship expressed in eq (18) and applied on eqs (10,11), one can obtain,

$$\begin{Bmatrix}\gamma_{axz}^{12}\\ \gamma_{ayz}^{12}\end{Bmatrix} = [B_{s12}]\{\delta\},\ \{w_1 - w_2\} = [B_{n12}]\{\delta\} \tag{22}$$

$$\begin{Bmatrix}\gamma_{axz}^{23}\\ \gamma_{ayz}^{23}\end{Bmatrix} = [B_{s23}]\{\delta\},\ \{w_2 - w_3\} = [B_{n23}]\{\delta\} \tag{23}$$

where the matrices $[B_{s12}]$, $[B_{n12}]$, $[B_{s23}]$ and $[B_{n23}]$ are derived using the shape functions for 8-nodes serendipity element.

By adopting the Gaussian quadrature formula eq (19) for eq (12), the stiffness matrices for the adhesive between the plates 1 and 2, and the plates 2 and 3 are respectively:

$$[K_{a12}] = t_a G_a \int_{-1}^{1}\int_{-1}^{1}[B_{s12}]^T[B_{s12}]\,det[J]\,d\xi\ d\eta + \frac{E_a}{t_a}\int_{-1}^{1}\int_{-1}^{1}[B_{n12}]^T[B_{n12}]\,det[J]\,d\xi\ d\eta \tag{24}$$

$$[K_{a23}] = t_a G_a \int_{-1}^{1}\int_{-1}^{1}[B_{s23}]^T[B_{s23}]\,det[J]\,d\xi\ d\eta + \frac{E_a}{t_a}\int_{-1}^{1}\int_{-1}^{1}[B_{n23}]^T[B_{n23}]\,det[J]\,d\xi\ d\eta \tag{25}$$

2.5.3 Plates Consistent Mass Matrices

To derive the mass matrix of each plate, we must also adopt the Gaussian quadrature formula by expressing the kinetic energy in the following form:

$$T_i = \frac{1}{2}\{\dot{\delta}_i\}^T [M_i]\{\dot{\delta}_i\} \tag{26}$$

The inertia effect associated with the rotational degrees of freedom has been assumed to be zero in equation (13). But in this case, the inertia effect is to be included. Hence, the mass moment of inertia of half of the beam segment about each end shall be computed and included at the diagonal locations corresponding to the rotational degrees of freedom. Thus, using the Gaussian quadrature formula eq (26) in eq (13) and including the inertia effect,

$$[M_i] = \int_{-1}^{1}\int_{-1}^{1}[F_i]^T[m_i][F_i]\,det[J]\,d\xi\ d\eta \tag{27}$$

where $[F_i]$ is a matrix function of the shape functions. [m_i] is found in [6]

2.5.4 Adhesive Mass Matrices

Using the nodal displacement relationships expressed in eqs (15, 16, 17) and the Gaussian quadrature eq (26) for eq (14), we get,

$$[M_{a12}]\ \rho_a t_a \int_{-1}^{1}\int_{-1}^{1}[L_{12}]^T[L_{12}]\,det[J]\,d\xi\ d\eta \tag{28}$$

$$\text{And}\quad [M_{a23}] = \rho_a t_a \int_{-1}^{1}\int_{-1}^{1}[L_{23}]^T[L_{23}]\,det[J]\,d\xi\ d\eta \tag{29}$$

where the matrices $[L_{12}]$, and $[L_{23}]$ are derived using the shape functions of 8-nodes serendipity element.

2.5.5 Assembly

The elementary mass and stiffness matrices are set in three categories as follows:
Before the overlap length ($0 \le x < L - a$),

$$[K^e]_1 = [K_1] + [K_3],\ [M^e]_1 = [M_1] + [M_3] \tag{30, 31}$$

At the overlap length ($L - a \leq x < L$),

$$[K^e]_2 = [K_1] + [K_2] + [K_3] + [K_{a12}] + [K_{a23}],\ [M^e]_2 = [M_1] + [M_2] + [M_3] + [M_{a12}] + [M_{a23}] \quad (32, 33)$$

After the overlap length ($L \leq x < 2L - a$),

$$[K^e]_3 = [K_2],\ [M^e]_3 = [M_2] \quad (34, 35)$$

Once the elementary mass and stiffness matrices are set for each element, their assembly will be made in global mass and stiffness matrices in order to take into consideration the whole displacements nodes in the structure.

2.5.6 Eigen problem resolution

Once the global mass and stiffness matrices are obtained, the following Eigen-equation corresponding to the problem can be solved for determining the natural frequencies (Ye and You [18]):

$$(-\omega^2[M] + [K])\{\Delta\} = 0 \quad (36)$$

The modes classification corresponds to the natural frequencies obtained in ascending order, from the lowest to the highest. The number of natural frequencies depends on the mesh size, and it is equal to the degree of freedom of the system. But the frequencies analysed are the ones corresponding to the first 10 modes classified from the lowest (fundamental) to the highest.

3 NUMERICAL VALIDATION

3.1 Mechanical and geometrical properties

The analytical model developed above is set and solved on MATLAB and the collected results are compared and validated with the ones obtained from numerical model simulation on ANSYS Workbench with a model based on the technique of finite element method (FEM); the considered mesh is an hexahedron element as shown in fig. 12a, with a 2.5 mm x 2.5 mm element surface size, giving a fast result with a high precision.

Three types of substrates were examined: structural steel, polyethylene (PE) and composite laminate constituted of 0.5 mm layers of UD glass-epoxy repeated with $0^0/90^0$ orientation; their mechanical properties are provided by the manufacturer and summarized in Tables 1 and 2. The adhesive was made of epoxy/resin material, and its mechanical properties are given in Table 1. Geometric properties of the double lap joint studied are shown in Table 3. As for the mesh size, a 1mm mesh length is enough to obtain accurate results; smaller meshes take more time to solve and converge to the results obtained for 1mm.

Properties	Steel	PE	Epoxy adhesive
Young's Modulus E (GPa)	200	1.1	0.5
Poisson's Ratio υ	0.3	0.42	0.35
Density ρ (kg/m^3)	7850	950	1595

Table 1: Isotropic properties of structural steel, polyethylene and epoxy adhesive.

Properties	Symbol	Value
Fibers' fraction volume	V_f	60%
Longitudinal Young's Modulus (GPa)	E_{11}	46
Transverse Young's Modulus (GPa)	E_{22}	10
In-plane shear Modulus (GPa)	G_{12}	4.6
In-plane Poisson ratio	υ_{12}	0.31
Density (kg/m^3)	ρ	2100

Table 2: Unidirectional properties of 60% glass fiber-epoxy.

Properties	Symbol	Value
Extreme plates' thickness (mm)	t_1	3
Middle plate thickness (mm)	t_2	6
Plates' width (mm)	b	30
Plates' length (mm)	L	100
Adhesive thickness (mm)	t_a	0.2
Overlap length (mm)	a	30

Table 3: Geometric parameters of DLJ.

3.2 Case of single fixed-free plate

First, modal analysis of a simple fixed-free plate is studied and the similar energy approach described for double lap-joint is used for only one plate and without adhesion. Results are obtained for different materials: Structural Steel, Polyethylene, glass fiber-epoxy laminate. The plate's geometric properties are t, b and L given in Table 3.

Modal analysis results are presented in figures 5, 6 and 7 showing the difference between the numerical models developed on ANSYS Workbench and the analytical model of section 2 for different substrates' materials. Results are close enough with an acceptable error for the first 10 modes: an error varying between 0.07% and 3.73% for structural steel, between 0.40% and 4.67% for polyethylene, and between 1.06% and 7.49% for the laminated glass fiber-epoxy. Hence, the model developed here is validated for single fixed-free plates.

3.3 Case of metallic substrates for DLJ

Fig. 8 shows a natural frequencies' comparison between the mathematical model solved on MATLAB and the numerical model of ANSYS Workbench for steel substrate. Maximum error of 11.08% is reached at mode 7. The relative error related to the fundamental frequency is 1.48%. The model is validated for structural steel.

3.4 Case of polymeric substrates for DLJ

Fig. 9 shows a natural frequencies' comparison between analytical and numerical models for polyethylene substrate. Maximum error of 42.24% is reached at mode 4. The relative error related to the fundamental frequency is 12.37%. The model is not validated for polymeric substrate.

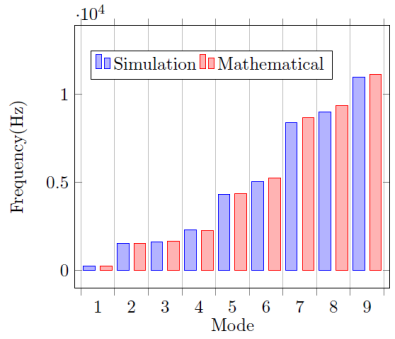

Figure 5. Natural Frequencies comparison between numerical and analytical model for fixed-free structural steel plate.

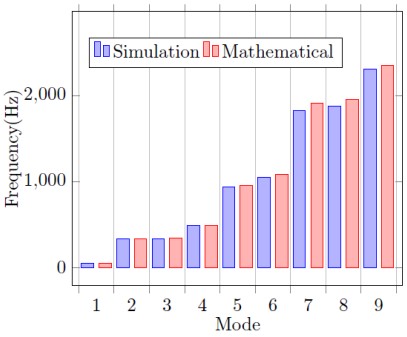

Figure 6. Natural Frequencies comparison between numerical and analytical model for fixed-free polyethylene plate.

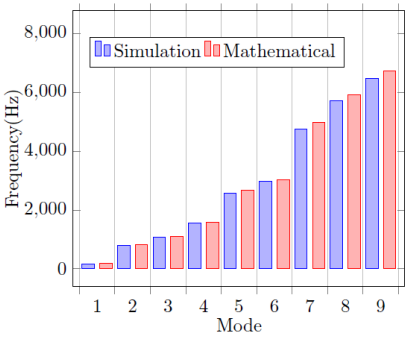

Figure 7. Natural Frequencies comparison between numerical and analytical model for fixed-free glass-epoxy composite plate.

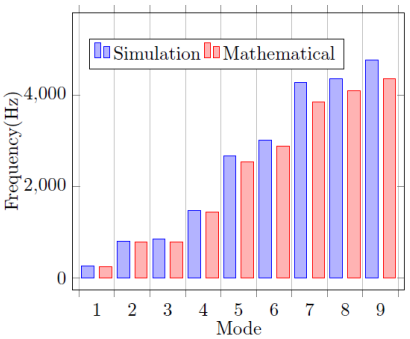

Figure 8. Natural Frequencies comparison between numerical and analytical models for DLJ structural steel structure.

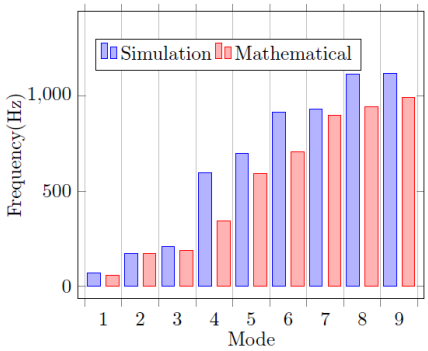

Figure 9. Natural Frequencies comparison between numerical and analytical model for DLJ polyethylene

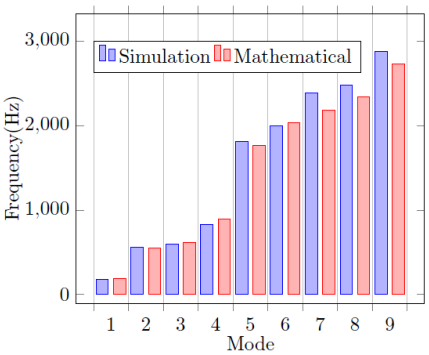

Figure 10. Natural Frequencies comparison between numerical and analytical models for DLJ composite.

3.5 Case of composite substrates for DLJ

Fig. 10 shows a natural frequencies' comparison between analytical and numerical models for composite substrate. Maximum error of 8.53% is reached at mode 7. The relative error related to the fundamental frequency is 3.53%. The model is validated for composite substrate.

3.6 Discussion

The analytical model described in this paper is validated for structural steel and composite laminate glass-epoxy, compared to the numerical model but not for polyethylene where the error reaches 42.04% at mode 4.

In fact, on one hand, assumption (5) leads to the following result: the displacements of the three plates are defined independently, but the adhesive's displacement between two plates is a function of the plates' displacement. This assumption is strictly rejected for the case of polyethylene because its transverse normal Young's modulus (1,100 MPa) is relatively close to that of the adhesive (500 MPa). Hence, the transverse normal deformation of the plates is not negligible in comparison with that of the adhesive and the displacements setup considered in the modelling do not respect the material's restrictions. This is not the case for structural steel material and the glass-epoxy composite where the transverse Young's Moduli are 200,000 MPa and 10,000 MPa respectively; the model is respected and this justifies the observations on the corresponding graphs where results are very close to the numerical model, with a maximum error of 11.08% for structural steel and 8.53% for glass-epoxy composite at mode 7, and small relative errors for the fundamental frequency: 1.48% for structural steel and 3.53% for glass-epoxy composite at mode 1.

On the other hand, assumption (5) is not considered in the case of fixed-free plate because no adhesion is introduced; hence, the model is validated for all substrates' materials, even for polypropylene.

The model developed above is also valid for any boundary conditions; the structure can exhibit any type of supports: fixed, simple or free supports at any point. The same solving procedure is adopted but boundary conditions must be taken into account; fixed points have zero displacement vector $\delta_i(x, y, t)$, simply supported points have zero angular displacement components $\psi_{ix}$and ψ_{iy} , and free points do not have any constrained displacement component.

4 EXPERIMENTAL ANALYSIS

The Impulse Excitation Technique (IET) is used essentially to measure the elastic moduli of a material as a function of measured sample's frequencies, mass and dimensions. The IET is non-destructive technique, with high precision and with which the elasticity moduli are easy to measure (Young's and shear moduli). It is used for a wide range of materials (ASTM E1876 [19]): metals, composites, ceramics, coatings …etc. for any temperature from ambient to high.

The principle of the IET is to measure the resonance frequencies of a sample impacted by an impulser. The excitations are performed automatically (by excitation unit) or manually. A specimen can be excited in different vibrational modes: longitudinal, flexural and torsional (Slim et al. [20-21]).

In this study, the measurement of vibration frequencies was done with the RFDA professional signal analysis system (Resonance Frequency and Damping Analysis) from IMCE Company (Genk, Belgium). Fig. 11 shows the experimental device giving the vibration frequencies of a sample excited in flexural mode. This equipment is equipped with an RFDA transducer, an excitation tool, a microphone with a frequency range up to 100 kHz, a support and a computer system equipped with RFDA software.

Before performing tests, the specimen was built in the support (Fig. 11). The recessed-free boundary conditions were adopted in our study. These mechanical excitations were carried out with a 6 mm diameter steel sphere glued to the end of a flexible 140 mm long polymer rod striking the upper surface of sample at its free end. The vibrations were detected by an acoustic microphone placed, under the free beam end, at 2-5 mm from the specimen surface.

The sample's vibrations are transformed by a transducer into electrical signals. They are amplified and processed by a signal analyser which gives the frequencies and period of sample vibration. The obtained signal in the time domain is treated in the frequency domain using the FFT in order to extract the resonance frequencies of the sample. This analysis was made by considering the lower and upper limits of signal respectively (5%, 95%). The measurements were repeated 20 times and the sample resonant frequencies were identified.

In this study, two adherents' materials will be considered (Steel and woven fabric 60% glass/polypropylene ASC) while the adhesive is epoxy AB glue. Table 1 in section 3.1 states the properties of steel and epoxy while table 4 shows the properties of ASC composite. For each case, two geometrical parameters, as shown in table 3, will be varied: Overlap length and thickness of the plates. Other parameters are kept constant: Adherents' length ($L = 100mm$), adherents' width: ($w = 30mm$), adhesive's material: resin/epoxy AB glue and adhesive's thickness ($t_a = 0.3mm$). Table 5 summarizes the different group of specimens' configurations to be tested.

Properties	Fibers' fraction volume	Young's Moduli (GPa)			Poisson Ratios			Shear Moduli (Gpa)			Density (kg/m^3)
Symbol	V_f	E_{11}	E_{22}	E_{33}	ν_{12}	ν_{13}	ν_{23}	G_{12}	G_{13}	G_{23}	ρ
Value	60%	13	13	3.54	0.08	0.14	0.14	1.25	1.52	1.52	1490

Table 4: Orthotropic properties of 60% glass fiber-polypropylene.

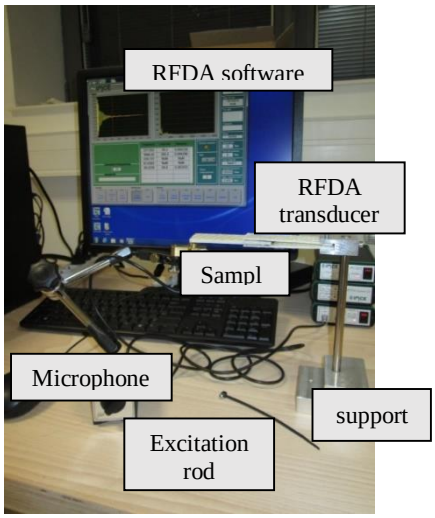

Figure 11. The device of Impulse Excitation Technique (IET).

Specimens	Adherents' Material	Adherents' thicknesses $t_1/t_2/t_1$ (mm)	Overlap length a (mm)
S1 (Ref.)	Structural Steel	1/2/1	30
S2	Structural Steel	1/2/1	50
S3	Structural Steel	1/2/1	80
S4	Structural Steel	1.5/3/1.5	30
S5	Structural Steel	2/4/2	30
C	ASC	1.5/3/1.5	30

Table 5: Configurations of tested specimens.

5 NUMERICAL SIMULATIONS

Before identifying and interpreting the experimental results, numerical simulation on ANSYS Workbench was developed in order to determine numerically the natural frequencies of the DLJ structure and compare the results with the experimental ones. The following assumptions were considered: Linear elastic material behaviour, small deflection theory and free vibration assumptions.

All geometric parameters defined earlier were integrated in the geometry module; materials properties defined in tables 1 and 4 (group S1) were modelled in a specific engineering data module. Fixed boundaries at the surface of the upper and the lower plates and mesh generation were defined in the model module. The considered mesh was a hexahedron element of dimensions and the mesh size was automatically generated (2.5*2.5*1 mm^3), giving good results with optimized time of resolution. Numerical simulation procedure is illustrated in fig. 12 for S1. Mode shapes of modes 1 to 4 are presented in fig. 13.

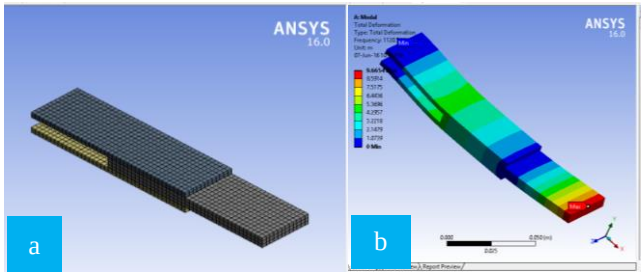

Figure 12. Numerical Simulation: (a) Mesh generation and (b) Total displacement.

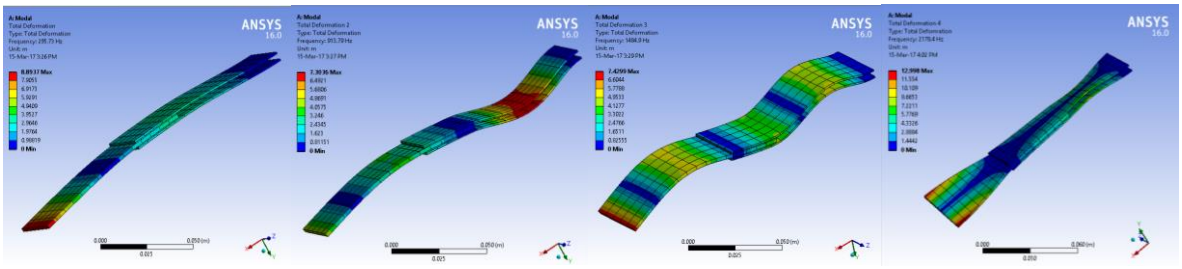

Figure 13. Four first Mode Shapes obtained for S1.

Specimens		S1	S2	S3	S4	S5	C
Mode 1	Num.	295.73	438.17	947.33	421.97	529.42	216.54
	Exp.	319	460	1019	398	507	198
Mode 2	Num.	913.79	1224.3	2640	1512	1666.6	700.34
	Exp.	943	1195	2357.9	1640	1617	650
Mode 3	Num.	1484.9	2238.9	3909.8	2150.4	2798.2	1106
	Exp.	1340	2400	3650	2197	2828	1105
Mode 4	Num.	1863.7	2914	5213	2720.9	3532.6	1886.5
	Exp.	1817	2590	5340	2760	3538	1780

Table 6: Natural frequencies in Hz obtained for different specimens.

Specimens	S1	S2	S3	S4	S5	C
Mode 1	7.87%	4.98%	7.57%	5.68%	4.23%	8.56%
Mode 2	3.20%	2.39%	10.69%	8.47%	2.98%	7.19%
Mode 3	9.76%	7.20%	6.64%	2.17%	1.06%	0.09%
Mode 4	2.51%	11.12%	2.44%	1.44%	0.15%	5.65%

Table 7: Relative error observed between numerical and experimental solutions.

6 RESULTS AND DISCUSSION

Tables 6 and 7 show respectively the natural frequencies and the relative error between the natural frequencies obtained from numerical simulation and experiments for each specimen. Experimental results show a good agreement with the numerical ones; the maximum error reached is 11%. Since the first column of table 7 (S1) shows an acceptable agreement between numerical model and experimental results, and according to the results obtained in section 3, the programmed analytical model will have the advantage to minimize hugely the time cost by finding the natural frequencies for all the rest of the configurations. The effect of adherents' thickness is shown in the fig. 14. It is obvious that the increase of thickness leads to an increase in stiffness much higher than the increase in mass thus the overall natural frequencies will increase. However when the thickness doubles from 2 mm to 4 mm the increment of natural frequency is bounded between 1.5 and 2 times. Hence the resonant frequency is more sensitive towards overlap ratio than plates' thickness. Fig. 15 shows the influence of overlap length on the resonant frequencies. Indeed, one may talk about overlap ratio which is the ratio of the overlap length to the length of the plate; in this study, three ratios were examined: 0.3, 0.5 and 0.8. When this ratio increases, the contact area between the substrates increases and hence the ''free length'' of each substrate will shorten and thus the stiffness increases which implies an increase in the natural frequencies. The frequencies increase almost three times when the overlap ratio varies from 0.3 to 0.8. Moreover, for a small value of overlap ratio of 0.3, the rate of increase of the frequency from mode to mode is higher than for the case of higher overlap ratios. For instance, the mode 2 frequency is three times the fundamental frequency for an overlap ratio of 0.3 while it is about 1.5 times for an overlap ratio of 0.8. The results of material's type influence on the resonance frequencies are presented in fig. 16. Neglecting the mass of the thin adhesive layer, the mass of steel specimen is about 141 g while the composite one weights around 27 g hence composite specimen is lighter 5 times but the steel substrates are stiffer by 15 times. This gap appears especially at lower modes (1 and 2) where the natural frequency for steel is almost twice. This ratio decreases for higher modes. The results of this study suggest a potential application in the field of structures assembly. For instance, if a light structure is needed with higher frequencies, we can configure a composite assembly with higher overlap ratio. If stress concentration at the edges is an issue, overlap could be reduced and the substrates' thickness increased instead.

7 CONCLUSION

In this paper, an analytical model based on energy formulation and elements discretization is established to calculate resonant frequencies of a double lap bonded joint. In addition, an experimental measurement of the natural frequencies of a fixed-free double lap bonded joints was carried out. 3D finite element numerical simulations were applied with ANSYS to validate both analytical and experimental analysis. This study approved the possibility to use the Impulse Excitation Technique to measure the frequencies of an assembled structure with a good accuracy. A good agreement was found where the maximum error is estimated to 11%. This might help to apply the established analytical model and save time in numerical calculations especially when it deals with parametric study. Three parameters were examined: substrates' materials, substrates thickness and overlap length. It was found that the overlap length has the main influence on the vibration frequencies of a DLJ structure. Increasing the overlap length and the plates' thicknesses led to increase the resonance frequencies of structure however this will lead to a negative effect towards singularity points at the adhesive layer edge. The resonance

frequencies of steel structure are more important than these of composite one however the total mass of the structure may play a crucial role in design. Finally, this study offers many configurations options of such assembly that could be designed in order to satisfy the technical requests of certain applications.

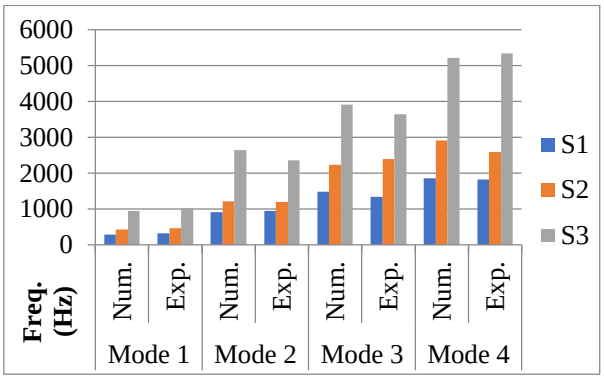

Figure 14. Comparison of resonant frequencies between S1, S2 and S3 (effect of adherents' thickness).

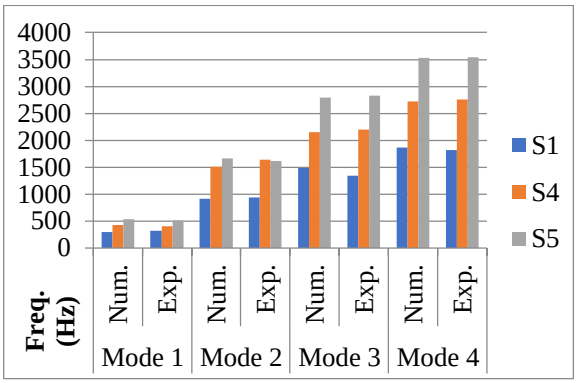

Figure 15. Resonant frequencies comparison between S1, S4 and S5 (influence of overlap length).

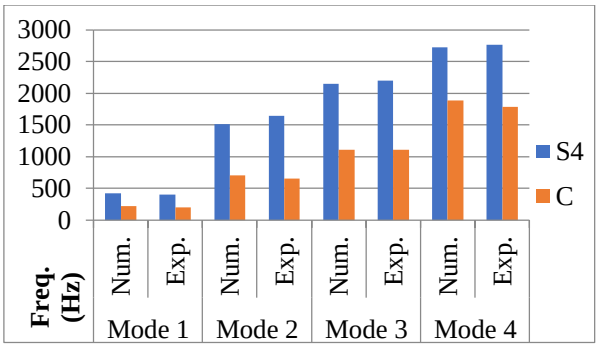

Figure 16. Resonant frequencies comparison between S4 and C (influence of material's type).

REFERENCES

[1] He S, Rao MD (1992). Vibration analysis of adhesively bonded lap joints, Part I: Theory. Journal of Sound and Vibration 152(3), 405-416.

[2] Khalil AA, Kagho AN (1991). Non-destructive testing of adhesively bonded joints using vibrational analysis. International Journal of Adhesion and Adhesives 11(2), 121-127.

[3] Ko TC, Lin CC, Chou RC (1995). Vibration of bonded laminated lap-joint plates using adhesive interface elements. Journal of Sound and Vibration 184(4), 567-583.

[4] Rao MD, He S (1992). Vibration analysis of adhesively bonded lap joints, Part II: Numerical solution. Journal of Sound and Vibration 152(3), 417-425.

[5] Saito H, Taini H (1984). Vibrations of bonded beams with single lap adhesive joint. Journal of Sound and Vibration 92(2), 299-309.

[6] He X, Oyadiji SO (2001). Influence of the adhesive characteristics on the transverse free vibration of single lap-jointed cantilevered beams. Journal of Materials Processing Technology 119, 366-373.

[7] He X (2014). Finite element analysis of torsional free vibration of adhesively bonded single-lap joints. International Journal of Adhesion and Adhesives 48, 59-66.

[8] Du Y, Shi L (2014). Effect of vibration fatigue on modal properties of single lap adhesive joints. International Journal of Adhesion and Adhesives 53, 72-79.

[9] Samaratunga D, Jha R, Gopalakrishnan S (2015). Wave propagation analysis in adhesively bonded composite joints using the wavelet spectral finite element method. Composite Structures 122, 271-283.

[10] Vaziri A, Hamidzadeh HR, Nayeb-Hashemi H (2001). Dynamic response of adhesively bonded single-lap joints with a void subjected to harmonic peeling load. Proccedings of the institution of mechanical engineers, Part K: J. Multiody. Dynamics 215, 199-206.

[11] Rao MD, Zhou H (1994). Vibration and damping of a bonded tubular lap joint. Journal of Sound and Vibration 178(5), 577-590.

[12] Vaziri A, Nayeb-Hashemi H (2002). Dynamic res`ponse of tubular joints with an annular void subjected to a harmonic axial load. International Journal of Adhesin and Adhesives 22, 367-373.

[13] Quing G, Feng Z, Liu Y, Qiu J (2006). A semianalytical solution for free vibration analysis of stiffened cylindrical shells. Journal of Mechanics of Materials and Structures 1(1), 129-145.
[14] Challita G, Othman R (2012). Analytical model of the double-lap bonded joints response to harmonic loads. European Journal of Mechanics A/Solids 34, 149-158.
[15] Al-Mitani K, Othman R (2016). Analytical solution of the harmonic response of visco-elastic adhesively bonded single-lap and double-lap joints. International Journal of Adhesion and Adhesives 71, 55–65.
[16] Jiang C, Heyliger PR (2017). Thickness effect in the free vibration of laminated magnetoelectroelastic plates. Journal of Mechanics of Materials and Structures 12(4), 521-544.
[17] Lin CC, Ko TC (1997). Free vibration of bonded plates. Composite Structures 64(1-4), 441-452.
[18] Yeh MK, You YL (1995). Vibration of laminated plates with adhesive joints. Composites Engineering 5(8), 983-993.
[19] ASTM E1876 (2015) Standard Test Method for Dynamic Young's Modulus, Shear Modulus and Poisson's ratio by Impulse Excitation of Vibration.
[20] Slim MF, Alhussein A, Billard A, Sanchette F, François M (2017). On the determination of Young's modulus of thin film with Impulse Excitation Technique. Journal of Materials Research 32(3), 497-511.
[21] Slim MF, Alhussein A, Sanchette F, Guelorget B, François M (2017). An enhanced formulation to determine Young's and shear moduli of thin films by means of Impulse Excitation Technique. Thin Solid Films 631, 172-179.